Comun. Inst. Geol. e Mineiro, 2001, t. 88, pp. 33-50

A 8

The Amares basin: an ENE-WSW graben formed by recent reactivation of the late-Variscan fracture network?

F. O. MARQUES*; A. MATEUS**; H. AMARAL***; M. A. GONÇALVES**; C. TASSINARI****; P. SILVA***** & J. M. MIRANDA*****

Key-words: Fracture network; Chronology; Variscan; Alpine; Amares Graben.

Abstract: A detailed knowledge of the fracture network in Portugal is needed for a better assessment of pollution risks, resources and quality of water, geotechnical and seismic hazard. With this motivation in mind, we carried out a detailed study of the fracture network in a granite-dominated area NE of Braga, NW Portugal.

The methodologies used in fracture detection included the geomorphologic analysis of topographic maps and digital terrain models, and the lineament interpretation in vertical aerial photographs and satellite imagery. This general interpretation, followed by detailed field structural characterization, revealed three main sub-vertical fracture systems: predominant E-W to ENE-WSW and NNW-SSE families, and a subsidiary N-S to NE-SW family. The older, hotter mineral fault infillings (mostly comprising coarser aggregates of quartz, muscovite and tourmaline) preserve kinematical criteria of dominant strike-slip movements – sinistral in the E-W to ENE-WSW system, and dextral in the NNW-SSE and N-S to NE-SW families. Age, geometry and kinematics suggest that the NNW and NNE systems represent the Variscan dextral conjugates of the sinistral E-W to ENE-WSW fault system. The younger, colder fault rocks (usually very fine fault gouges) indicate dominant dip slip movement in all the observed fault systems.

AMS studies were also performed to evaluate deformation within granite rocks. The obtained data show that ductile deformation of granite is localized and related to the earliest displacements accommodated by major fault zones. Isotope dating (K/Ar) of muscovite from fault surfaces and an aplite dyke intruded into a NE-SW fault zone point to a minimum age of *ca.* 312 Ma for the earliest faulting event. The age of the colder, younger reactivation was constrained only by geomorphology and tectonics. Well-preserved geomorphologic features (*e. g.,* flat bottom and well-preserved flats, arranged in steps, bounded by dip-slip vertical faults in the graben bounding slopes) and present knowledge of the Alpine stress field, suggest that the basin is tectonic (graben) and recent (at least reactivated since Late Miocene). Geometry and youngest kinematics of all fracture systems, together with the approximately ENE-WSW elongation of the graben, suggest that it can result from extension in the outer arc of buckled lithosphere during recent NNW-SSE compression.

Palavras-chave: Rede de fracturação; Cronologia; Varisco; Alpino; Graben de Amares.

Resumo: Para uma melhor avaliação dos riscos de poluição, recursos e qualidade da água, e casualidades geotécnicas e sísmicas, torna-se necessário um conhecimento detalhado da rede da fracturação em Portugal. Com esta motivação em mente, procedeu-se a um estudo detalhado da rede de fracturação numa área dominada por granitos a NE de Braga, NW de Portugal.

As metodologias utilizadas na detecção de fracturas incluíam a análise geomorfológica em mapas topográficos e modelos digitais de terreno, e a interpretação de lineamentos em fotografias aéreas verticais e imagens de satélite. Esta interpretação geral, seguida de caracterização estrutural detalhada no campo, revelou três sistemas principais de fracturas subverticais: duas famílias predominantes, E-W a ENE-WSW e NNW-SSE, e um sistema subsidiário N-S a NE-SW. Os preenchimentos minerais de falha mais antigos e de mais alta temperatura (sobretudo agregados de quartzo mais grosseiro, turmalina e muscovite) preservam critérios de movimento predominantemente de desligamento – esquerdo no sistema E-W a ENE-WSW, e direito nas famílias NNW-SSE e N-S a NE-SW. A idade, a geometria e a cinemática sugerem que os sistemas NNW e NNE representem os conjugados direitos variscos do sistema esquerdo E-W a ENE-WSW. As rochas de falha mais jovens e de mais baixa temperatura (normalmente farinhas de falha muito finas) indicam um movimento dominante de "*dip slip*" em todos os sistemas de falhas observados.

Realizaram-se também estudos de ASM para avaliação da deformação em rochas graníticas. Os dados obtidos mostram deformação dúctil do granito localizada e relacionada com movimentos mais precoces acomodados por zonas de falha principais. A datação isotópica (K/Ar) de concentrados de muscovite de superfícies de falha e de um dique aplítico intruído numa falha NE-SW aponta para uma idade mínima de cerca de 312 Ma para o evento mais precoce de fracturação. A idade da reactivação mais fria e mais jovem foi constrangida pela geomorfologia e pela tectónica. Elementos geomorfológicos bem preservados (*e. g.*, fundo chato e patamares, dispostos em degrau, limitados por falhas subverticais com movimentação em "*dip slip*" nas vertentes que limitam o *graben*) e o actual conhecimento do campo de tensões alpino sugerem que a bacia de Amares seja tectónica (*graben*) e recente (pelo menos reactivada desde o Miocénico superior). A geometria e a cinemática mais recente de todos os sistemas de fracturas, conjuntamente com o alongamento ENE-WSW do *graben*, sugerem que este possa resultar de extensão no arco externo de litosfera arqueada durante compressão NNW-SSE recente.

* LATTEX, Dep. Geologia, FCUL, Edifício C2, Piso 5, 1749-016 Lisboa, Portugal.
** CREMINER, Dep. Geologia, FCUL, Edifício C2, Piso 5, 1749-016 Lisboa, Portugal.
*** Research Project DIWASTE, Fundação da FCUL, Edifício C4, Piso 3, 1749-016 Lisboa, Portugal.
**** Instituto de Geociências, Universidade de São Paulo, Brasil.
***** CeGUL, Dep. Física, FCUL, Edifício C8, Piso 5, 1749-016 Lisboa, Portugal.

INTRODUCTION

Data regarding the geometry and kinematics of major (regional) fault zones in Northern Portugal have been commonly used to interpret the Late-Variscan fracture network as a structural pattern mainly involving two main fault systems formed during two main events (RIBEIRO, 1974; RIBEIRO *et al.*, 1979): a dominant, sinistral strike-slip, N-S to NNE-SSW system, conjugate to a less developed, dextral strike-slip, NNW-SSE family, generated during a N-S compressive event dated between 300 and 280 Ma (RIBEIRO *et al.*, 1979); a later E-W compressive event was dated between the Autunien and the lower Triassic (280 to 220? Ma), during which some pre-existing fault zones were reactivated with a significant inverse component of displacement (*e. g.* the Porto-Tomar shear zone; RIBEIRO *et al.*, 1980).

For the Montesinho region (NE Portugal), PEREIRA *et al.* (1984) defined two late Devonian (post 395 Ma) fault systems – a dextral N-S ± 15° and a sinistral E-W ± 15° – and two post-Stephanian (post 295 Ma) fault systems – N-S to NNE-SSW faults reactivated as sinistral coupled with the generation of a conjugate dextral WNW-ESE system. In a more recent work, PEREIRA *et al.* (1993) considered as a whole the main Late-Variscan fracture network of the Portuguese inland and defined two conjugate strike-slip fault systems developed during the Permian (280-230 Ma) – a sinistral NNE-SSW to NE-SW system and a dextral NW-SE system. From the geometry and kinematics of the conjugate fault systems, PEREIRA *et al.* (1993) deduced a significant anticlockwise rotation of the stress field relative to earlier Variscan deformation. Despite all these structural studies and kinematical interpretations, insufficient efforts have been made to characterise the fault rocks and/or the hydrothermal mineral precipitates that often are found in many fault segments. Such studies could fully constrain the relative chronology and the main active processes involved in fracturing (generation and/or reactivation) in NW Iberia during Late-Variscan times.

The neotectonic activity in N Portugal was synthesized by CABRAL (1995), and the evaluation of the vertical movements that took place in Upper Pliocene and Quaternary times shows that the NW domain of the Hesperian Massif was uplifted between 400 and 500 m, the Iberian Meseta reaching the present-day maximum altitude of *ca.* 800 m. This is mainly due to convergence between the African and the Eurasian plates in a direction approximately NNW-SSE to NW-SE that occurs in the eastern segment of the Açores-Gibraltar plate boundary (RIBEIRO *et al.*, 1996, and references therein).

To our knowledge, the importance of the ENE-WSW to E-W fracture system, as one of the most penetrative and as the Variscan sinistral conjugate to the dextral NNE-SSW system, has never received due attention in the published literature. Recently, MARQUES (1994) and MATEUS *et al.* (1999) mapped this system in restricted areas of NE Trás-os-Montes (Bragança Massif and S^{ta} Comba da Vilariça – Pocinho regions, respectively, covering together about 450 km^2) and recognised its importance in other sectors of north Portugal (Carvalhelhos, Vilarelho da Raia-Chaves, Sandim-Segirei, Serra da Estrela, Penedono-Celorico da Beira). According to the data meanwhile obtained, MARQUES & MATEUS (1998) suggested that NW to NE dextral families were the Variscan conjugates of the sinistral ENE to ESE fracture families.

From the above, it is clear that a greater and more detailed knowledge of the fracture network in Portugal is needed for a better assessment of pollution risks, resources and quality of water, geotechnical and seismic risk. We now present a detailed study of the fracture network carried out in an area of about 100 km^2 NE of Braga, Northern Portugal (Fig. 1). This area is characterized by the presence of biotite porphyroid granites, dated at *ca.* 318 Ma by U/Pb, with minor metasediments. A striking feature of the available published geological map (Fig. 2A) is the scarcity of faults, despite the conspicuous amount of lineaments observed in topographic maps (conventional or shaded relief – Fig. 2B) and vertical aerial photographs.

Besides the classical detailed structural analysis of fractures (geometry and kinematics), we have paid special attention to the different types of fault rocks, because their mineralogical nature and micro structural characteristics can be used to establish a relative chronology of the fault movements and to unravel some of the physical-chemical parameters that strongly control strain accommodation.

The Late Variscan fault zones now observed at the earth's surface, formed deep in the crust, contemporaneous with an over-thickened and heated crust (before and during post-collisional isostatic rebound) (MARQUES & MATEUS, 1998; MATEUS *et al.*, 1999). Thus, they often show mylonites, protomylonites and/or ultracataclasites of distinct lithological nature, besides high to medium temperature (≈ 400-200° C) fault mineral infillings, largely dominated by quartz aggregates that frequently

Fig. 1 – Location of the study area.

display microstructures ascribable to significant work hardening followed by dynamic recovery (*e. g.* MATEUS, 1995, MATEUS *et al.*, 1995 and references therein). The Variscan brittle crust cannot presently be observed in its central domain because it was removed by erosion during the post-collisional Variscan isostatic rebound. On the contrary, the Alpine compressive reactivation of the Late Variscan network now observed at the surface, caught these fractures at a high, cold crustal level, and thus fault rocks reflect these conditions (MARQUES & MATEUS, 1998; MATEUS *et al.*, 1999).

The age of the Variscan fracture events in Portugal has been typically evaluated by correlation with regional deformation and/or age of granites cut by faults (*e. g.*, RIBEIRO, 1974; RIBEIRO *et al.*, 1979; PEREIRA *et al.*, 1984; PEREIRA *et al.*, 1993). In the present study, the age of some faults was estimated by isotope dating. We used the K/Ar system to date muscovite concentrates from fault surfaces and from an aplite dyke intruded into a NE-SW dextral strike-slip fault. The age of the colder, younger reactivation was constrained only by geomorphology and tectonics. We did not carry out palaeontological, mineralogical or petrologic studies of sediments within the Amares basin to better constrain the age of its evolution. Correlation with other basins (grabens) of the NW of the Iberian Peninsula is not straightforward. These are mostly described as pull-apart basins related with Alpine strike-slip movements (*e. g.*, RIBEIRO, 1984; CABRAL, 1989, 1995; MARTÍN-SERRANO *et al.*, 1996; CABRERA *et al.*, 1996; MONTEIRO SANTOS *et al.*, 1999), which does not seem to be the case of the Amares basin (dip-slip kinematics in all fault systems bounding the basin).

We have used two main methodologies in fracture detection: (1) the geomorphologic analysis of topographic maps (1:25 000) combined with digital terrain models (shaded relief – 1:25 000), and (2) lineament interpretation in vertical aerial photographs (*ca.* 1:15 000), satellite imagery and again digital terrain models (Fig. 3). Geomorphologic analysis was also used in the evaluation of the age of graben formation, through the degree of preservation of features like flats arranged in steps bounded by faults, in the flanks of the graben, mostly, and flat bottom of the graben also. Image interpretation was followed by fieldwork for lineament confirmation and detailed structural analysis of the fracture network.

A

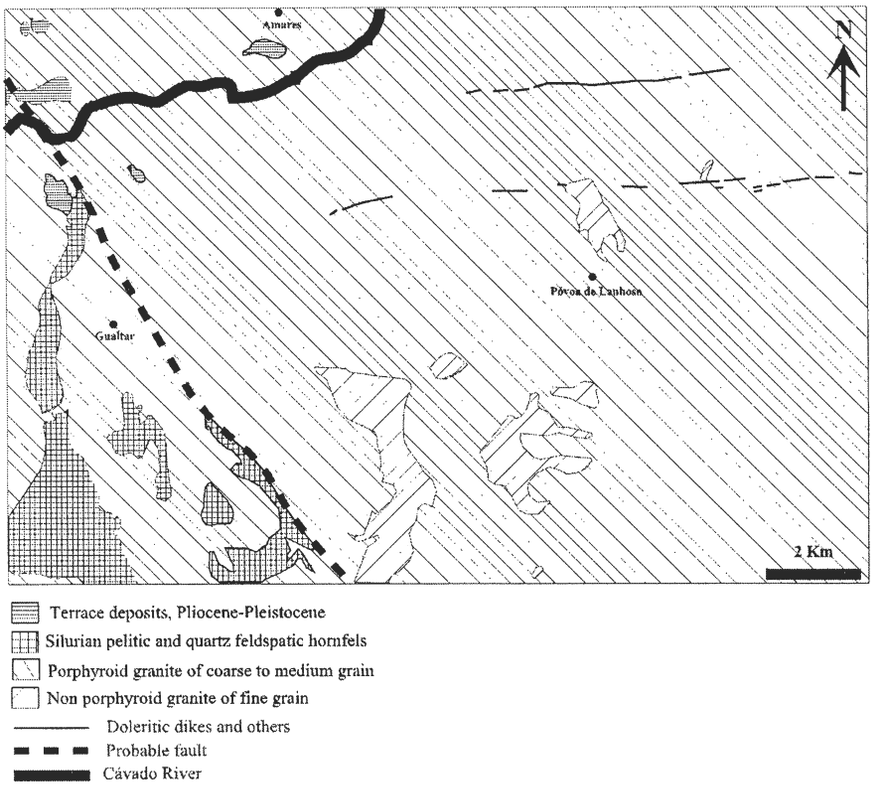

B

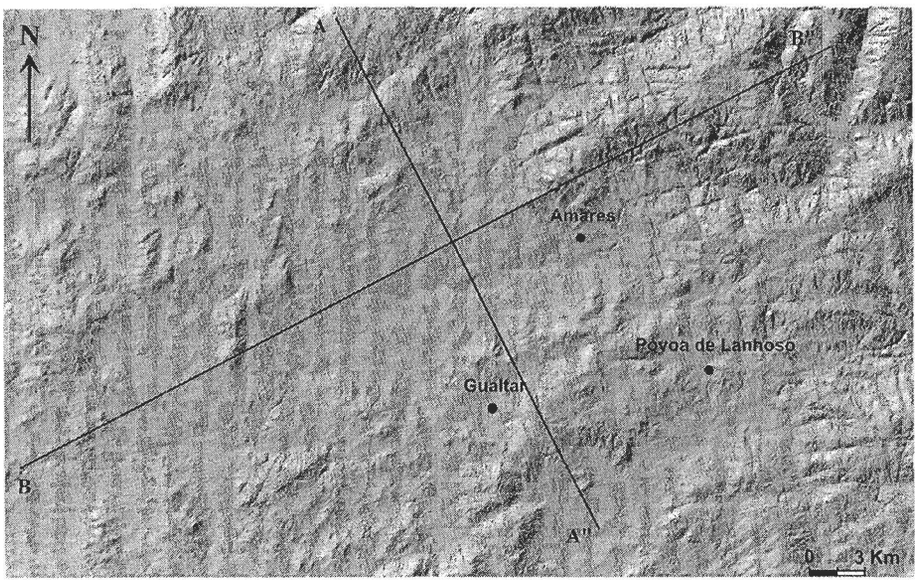

Fig 2 – A – Geological map adapted from Instituto Geológico e Mineiro publication.
B – Corresponding image of shaded relief. Note the contrast between the almost non-mapped faults in A and the abundance of lineaments in B, which correspond to fault zones (mostly) as shown by the present study. Both images were reduced to fit the page.

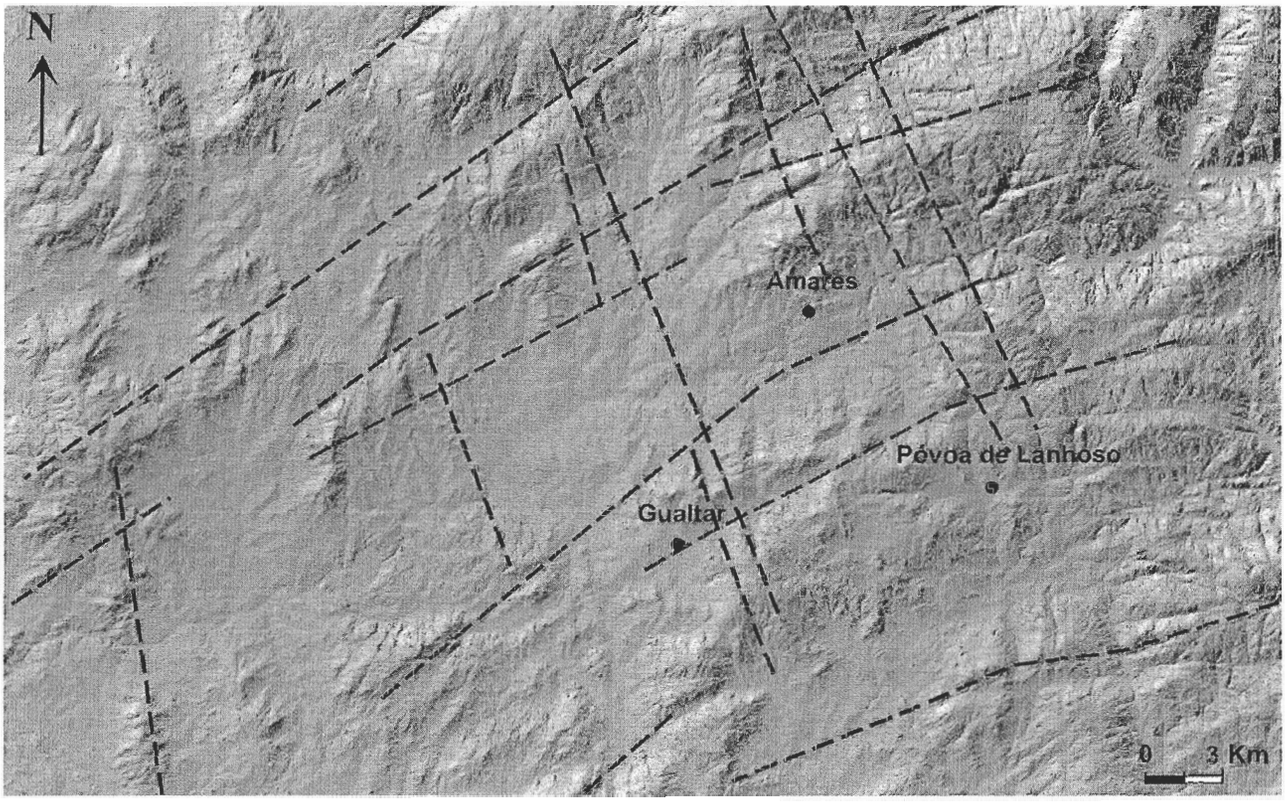

Fig. 3 – Vertical view of the shaded relief with incomplete lineament interpretation.

Finally, we used AMS techniques to characterize granite fabrics developed synchronously with the earliest displacements accommodated by the major fault zones, thus representing the older fracturing events.

DATA

Fault rocks and hydrothermal mineral fault infillings

Fault rocks formed during the earlier (ductile or semi-ductile) stages of shearing and mineral fault precipitates ascribable to hydrothermal activity under relatively high to medium temperature conditions are not very common in the study area, conversely to those generated during the later, brittle, and low-T reactivation events.

The earlier, most common mineral precipitates identified along many segments of major fault zones comprise aggregates of greyish milky quartz, sometimes coupled by significant amounts of muscovite and tourmaline. Usually, quartz grains of these aggregates display strong wavy extinction, deformation bands and serrated inter-granular boundaries; evidence of inter- and/or intra-granular sub-granulation can be found in some samples. When significantly rich in muscovite and tourmaline, these mineral precipitates show another type of quartz that generally occurs as elongated fibres, recording coeval strike-slip fault movements (see below). In these cases, muscovite sheets show only incipient bend gliding and typically define a conspicuous fabric that, regularly, is reinforced by the alignment (following the *c* axis direction) of prismatic, locally brittle deformed, crystals of tourmaline. The deposition of this mineral association, being coeval with the first fracturing stages within the biotite porphyry granite, documents the circulation of late-magmatic, silica saturated and boron enriched aqueous fluids under minimum temperatures of about 400 ± 50º C. It represents, probably, the waning stages of the igneous activity nearly contemporaneous with the aplite dykes emplacement along the major NE-SW structures.

Further fluid channelling, correlative of subsequent reactivation events of many fault zone segments, should not involve large volumes of hydrothermal solutions, since there is no evidence of significant mineral and textural transformations of the host granites. Episodic fluid focusing towards the reactivated fault segments under minimum temperatures ranging from near 300° to 250° C are, however, effective enough to promote the precipitation of milky quartz + chlorite ± sulphides (mostly pyrite) and, consequently, to induce partial replacement of the earlier muscovite into fine aggregates of illite. Grains of this new quartz generation are usually free of optical effects ascribable to plastic yielding, although they may record significant inter- and trans-granular fracturing. Chlorite ± pyrite deposition seems to occur later, sealing preferentially small fault surface depressions adjoining the jutting-outs carved in quartz aggregates. The overall arrangement of the crystallographic oriented chlorite sheets preserve, therefore, the strike-slip fault movements synchronous of their development (see below).

The geological record concerning the later reactivation events experienced by the mapped fault zones comprises intense cataclasis of previous mineral infillings and/or granite, coupled by intense and long-lived circulation of low-temperature aqueous fluids that lead to the development of massive clay-gouges with disseminated crushed quartz grains and accessory amounts of iron-(hydro-)oxides. Since a detailed characterization of the mineralogical nature of these clay-gouges is missing, a maximum temperature of 150° C represents the best estimate for their formation. Nevertheless, it is worth noting that the generation of these fault rocks implies either the circulation of fluids chemically very distinct of those responsible for the formation of earlier mineral fault infillings or a quite different tectonic regime of strain accommodation. The common kinematical criteria preserved in these fault rocks do not result therefore from textural arrangements intimately related to the preferred orientation of neo-formed minerals, but instead from the orientation of cold striations carved in the clay-gouges due to friction and dragging along the fault surface.

Structural

Geometry

The mapping of the fault network is presented in Fig. 4 and the geometrical characterization of fractures summarized in the stereographic plots of Fig. 5. The contoured projection of Fig. 5A reveals the existence of four main sub-vertical fault systems: N 70 ± 15°, N 0 ± 5°,

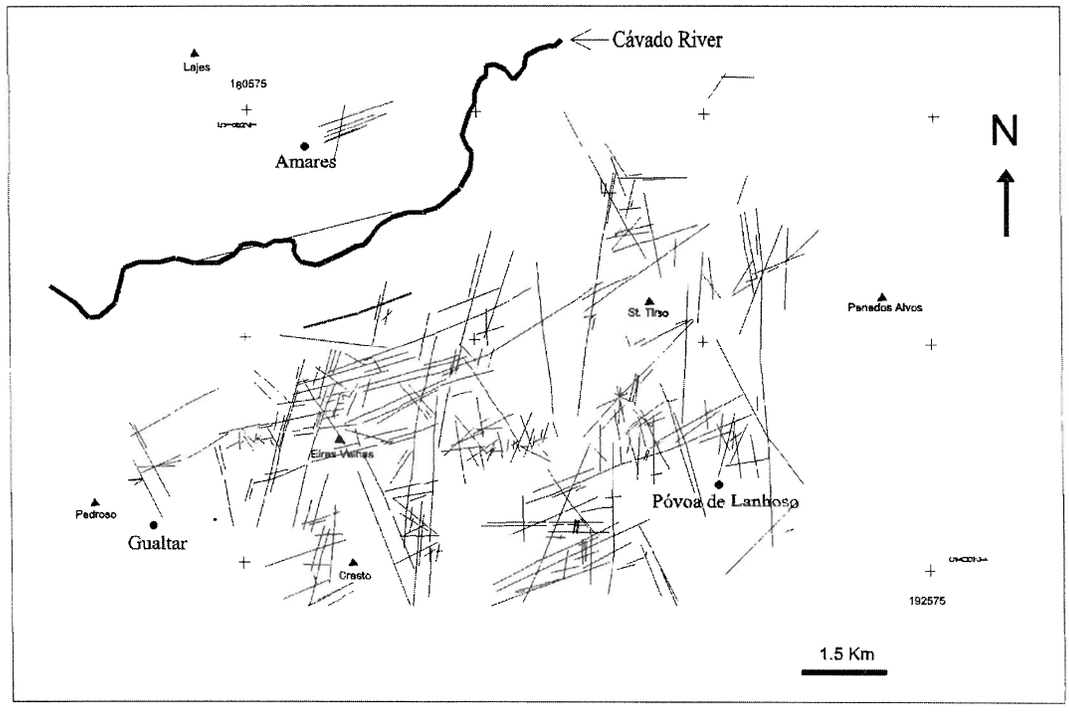

Fig. 4 – Mapped fault network in the Gualtar-Amares-Póvoa de Lanhoso region.

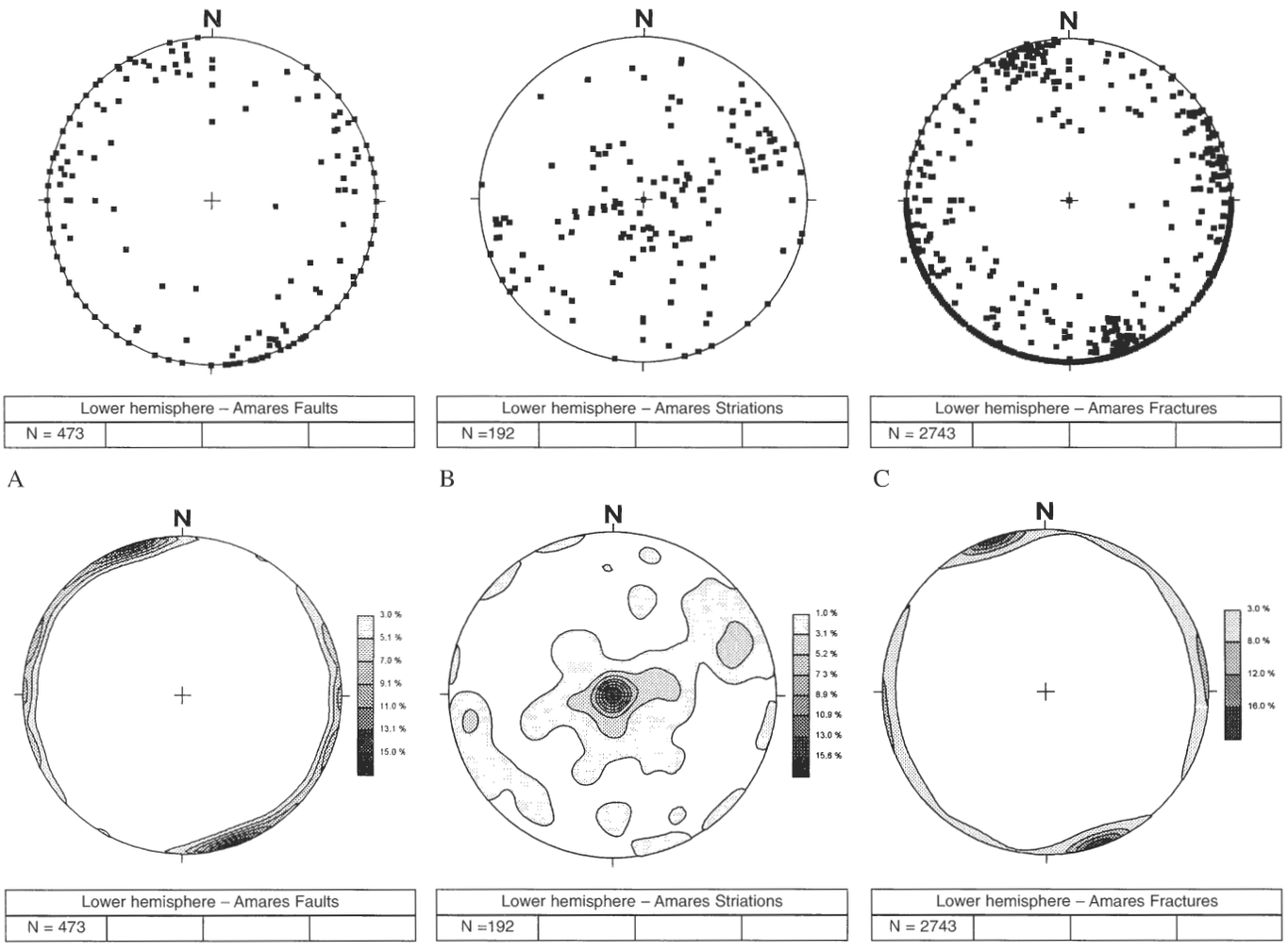

Fig. 5 – Stereographic plots and statistics of the studied fracture network.
A – Poles to fault planes; B – Fault striations and mineral fibres; C – Poles to fractures.

N 20 ± 10° and N 160 ± 10°. Not all the observed fractures plotted in Fig. 5C show clear evidence of movement parallel to the fracture surface (*i. e.*, not all are faults), although they can be sometimes filled with mineral aggregates, mostly quartz.

Slip data represented in the stereographic plots of Fig. 5B show two distinct distributions: the steeply dipping cluster corresponds to cold striations and the gently dipping to hot fibres (mostly quartz, but also muscovite and tourmaline).

The morphology of the graben is very well preserved (Fig. 6). Faults bounding the graben limit flats defining steps along the flanking slopes. The northern, southern and eastern flanking slopes of the graben are prominent; on the contrary, the western termination of the graben is not so clear, and faults seem to limit a small horst that separates the Amares graben from another graben to the WSW. The Amares graben has a flat bottom where the Cávado River meanders.

Kinematics

We have used the classic shear criteria to evaluate fault kinematics (Fig. 7A and B), and we have distinguished between the kinematics observed in "hot" fault mineral infillings and in "cold" clay-gouges. Shear criteria in the older mineral precipitates indicate a dextral strike-slip movement in the N 150 and N 0 to N 45 systems, and a sinistral strike-slip movement in the N 60 to N 90 system. Shear criteria preserved in fault gouges always indicate vertical movements.

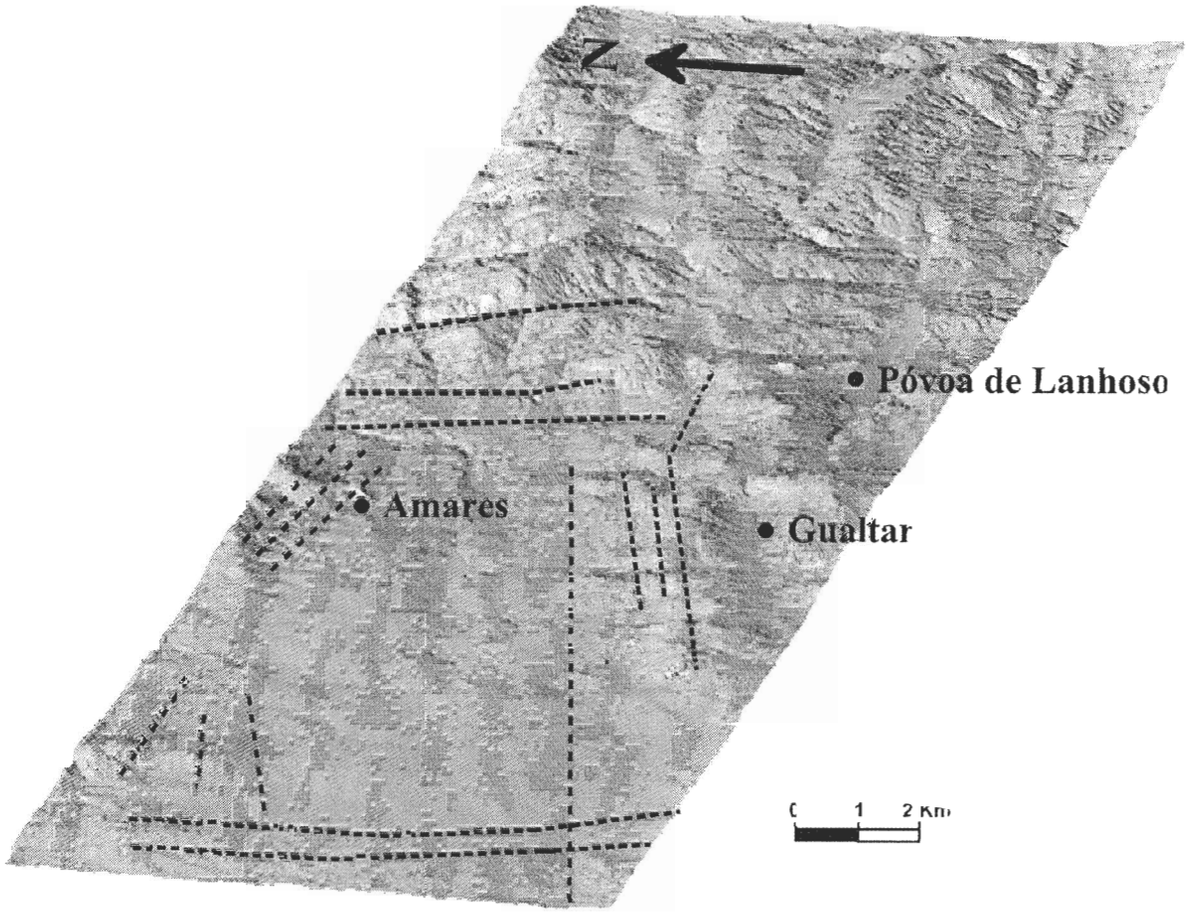

Fig. 6 – A – Oblique view of digital terrain model of the Amares graben with traces of major bordering faults.

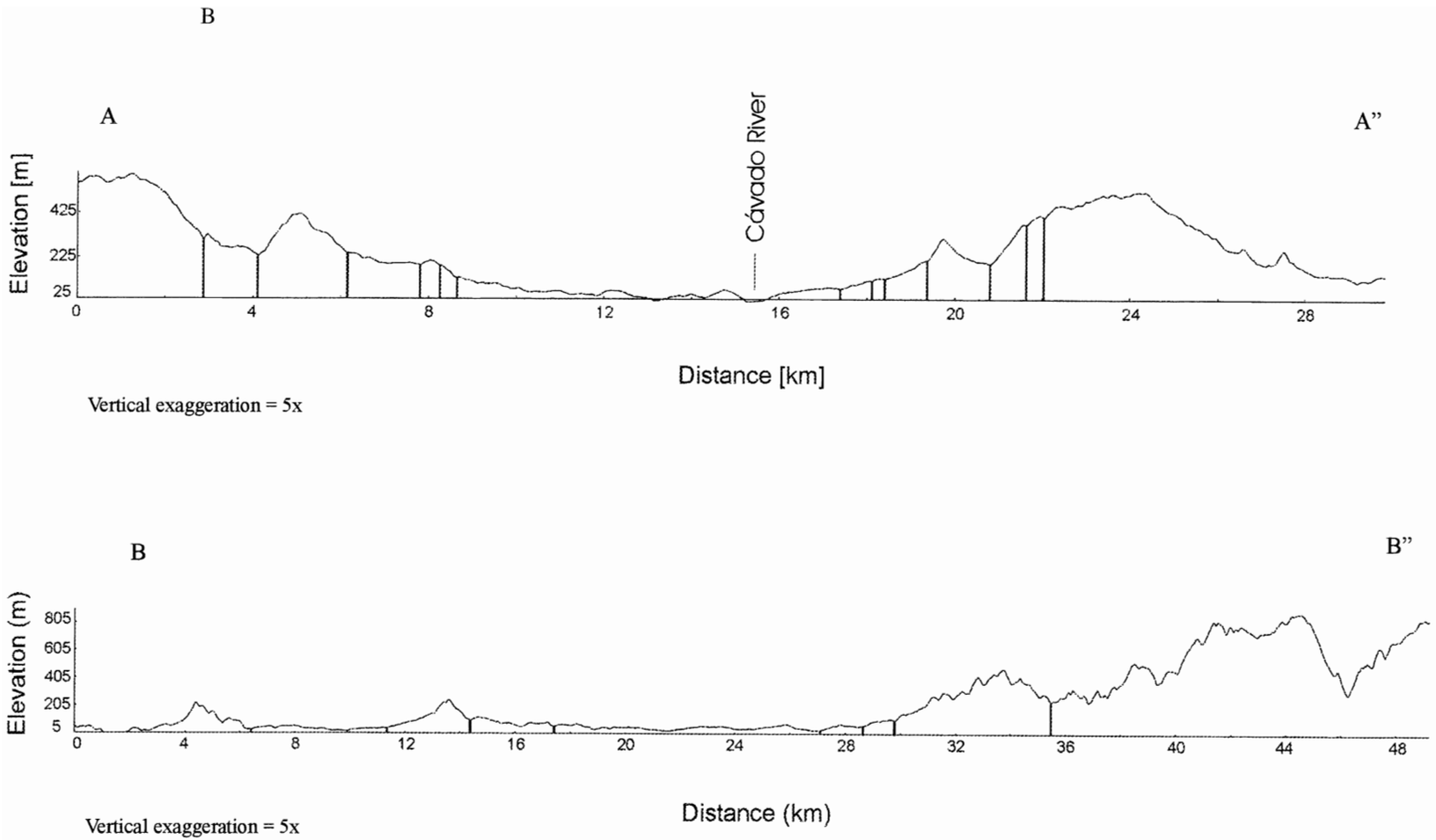

Fig. 6 – B – Topographic profiles (marked in Fig. 2B); vertical traces represent fault zones.

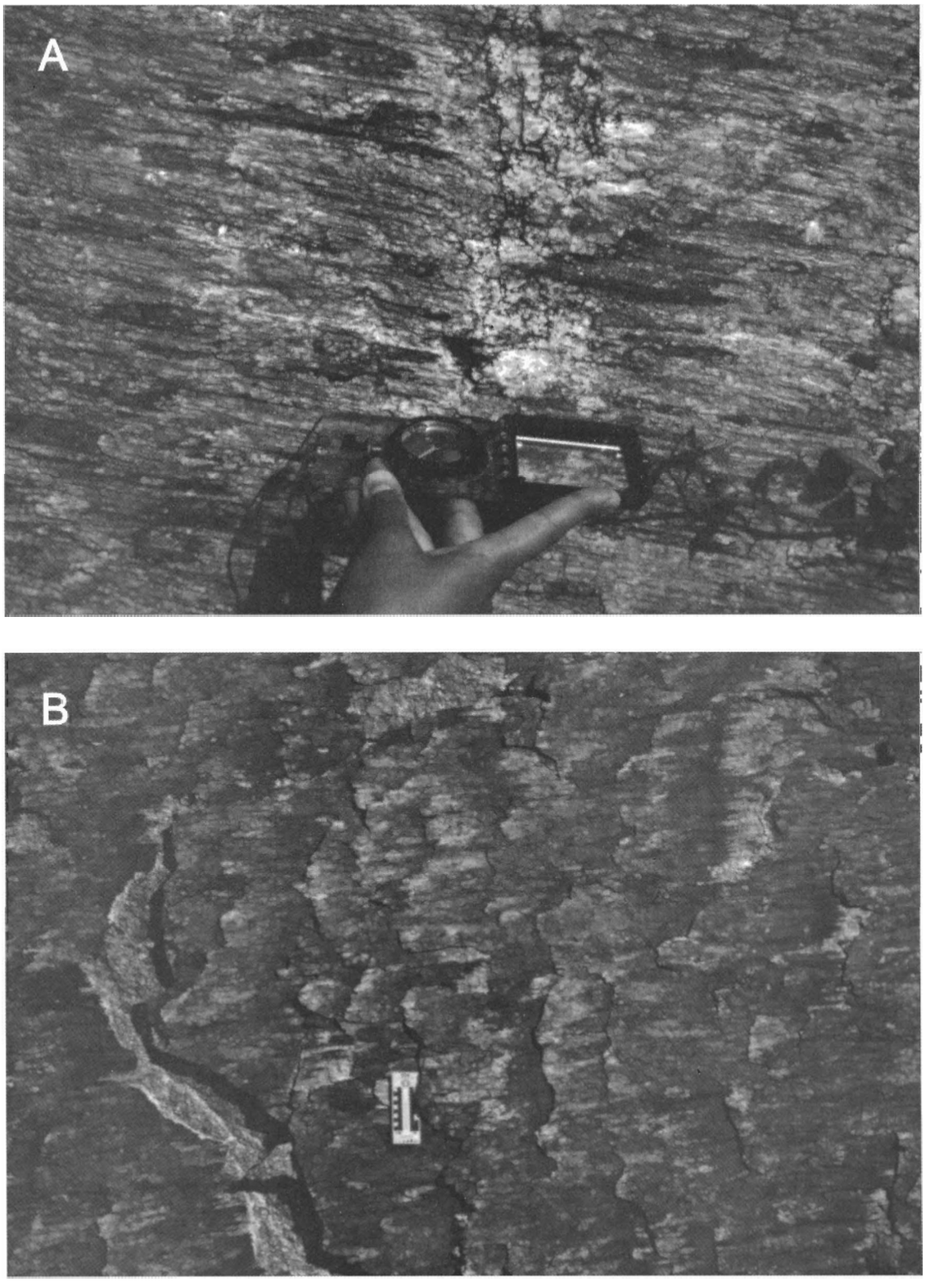

Fig. 7 – A – Photo of vertical NE-SW fault with muscovite and tourmaline infilling; the unusually long crystals of tourmaline are the kinematical marker.
B – Dextral shear criteria in vertical NE-SW fault. NE is to the right in both images.

Geochronology

Relative chronology

We used the estimated temperature conditions of formation of fault mineral infillings and fault rocks development to establish the relative chronology of fault movements. Given the thermal evolution of the Variscan belt in its late stages (early peak metamorphic conditions followed by a significant rising of the geotherms in the first 20-30 Ma of the post-collisional isostatic rebound – from *ca.* 300 to 270 Ma –, after which an important cooling of the upper/intermediate part of the crust took place), one concludes that fault segments with preserved high temperature mineral infillings are older than those with "cold" fault rocks. Because Alpine compressive events affected an isostatically rebounded crust ("hot" rocks were faster brought to shallow crustal levels), one finds, at the present day, "hot", older fault mineral infillings reactivated by "cold", cataclastic faulting, in the form of clay-gouges. Alpine compressive "hot" fracturing seats deep in the crust and cannot be directly observed. Therefore, the earlier fault mineral infillings (quartz + muscovite + tourmaline and quartz + chlorite ± illite ± pyrite) are Variscan in age, being the development of the clay-gouges ascribable to the seismic events that occurred during the Alpine compressive phases.

Isotope chronology

The K-Ar age determinations were conducted at the Geochronological Research Center of the University of São Paulo using the techniques described by AMARAL *et al.* (1966) with modifications. The K analysis was performed by flame photometry with a Micronal B-262 apparatus using a lithium internal standard. The Ar extraction was made in a high vacuum system with pressure usually less than 10^{-7} mm/Hg. Isotopic analysis of the purified argon was made in a MS-1 Nuclide mass spectrometer, now fully upgraded. All ages were calculated with the decay constants recommended by STEIGER & JAEGER (1977) and are given with standard error (1σ) estimates. The constants used in the calculations are:

$\lambda\beta = 4.962 \times 10^{-10}$ year^{-1}
$\lambda\kappa = 0.581 \times 10^{-10}$ year^{-1}
$(^{40}Ar/^{36}Ar)$ atm = 295.5
$^{40}K = 0.01167$ % K_{total}

Analytical data are presented in Table 1. K-Ar analysis performed on two muscovite samples from fault surface and from aplite dyke intruded in fault yield ages of 311 ± 10 Ma and 312 ± 7 Ma, respectively. Both results are in good agreement within analytical uncertainties, and can be interpreted as cooling ages of the dated minerals. The age of *ca.* 311 Ma probably dates the time of muscovite formation and is thus considered as a minimum age boundary for the fracturing episode.

AMS

A total of 88 samples were collected in granites from 3 sites – Pedreira de Seca (PS), Pedreira de Póvoa de Lanhoso (PL) and Pedreira de Calvos (CAL). These samples were analyzed in terms of the magnetic fabric, using AMS (Anisotropy of the Magnetic Susceptibility) techniques. This method revealed magnetic lineations and foliations not observed by conventional geological methods.

The determination of the magnetic fabric was made using a Kappabridge KLY-2 (Agico, Brno) susceptibility bridge, operating at a fixed frequency of 920 Hz, with an applied field of 0.1 mT. To characterize the anisotropy of the magnetic ellipsoid for the different samples, we used the Jelinek's parameters (JELINEK, 1981) (see TARLING & HROUDA, 1993 for details). The principal axes of the magnetic susceptibility ellipsoid are defined as $K_1 \geq K_2 \geq K_3$. Directional analysis for

TABLE 1
Analytical data of K/Ar isotope dating

SPK	Field Reference	Analysed Material	Rock	% K	^{40}ArRad CcSTP/g (*10-6)	^{40}ArAtm (%)	Age (Ma)	Maximum error (Ma)
7768	H9 A94	Muscovite	Fault surface	7.3952	97.54	5.43	311	10
7767	H9-Ap A94	Muscovite	Aplite	5.7240	75.81	5.54	312	7

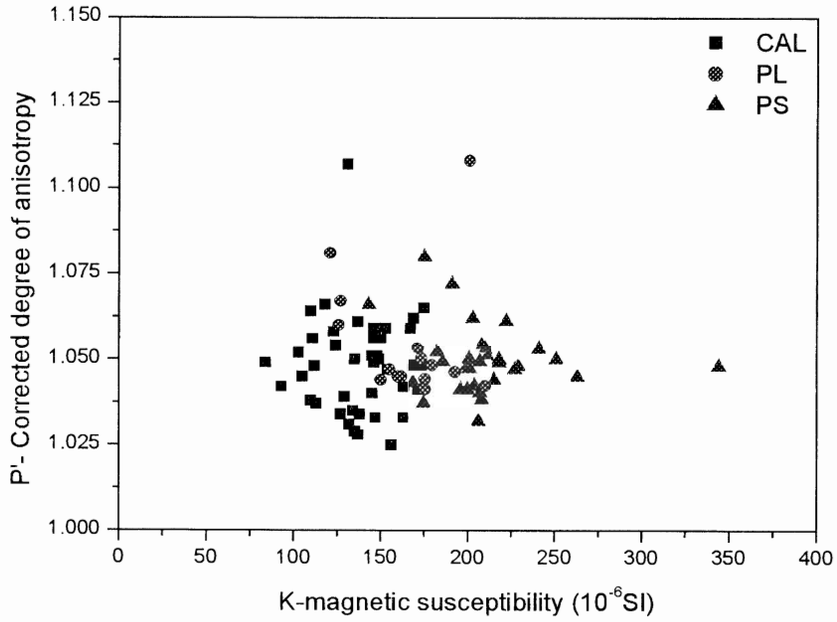

Fig. 8 – Distribution of bulk magnetic susceptibility values *versus* corrected degree of anisotropy, for the three sampled sites.

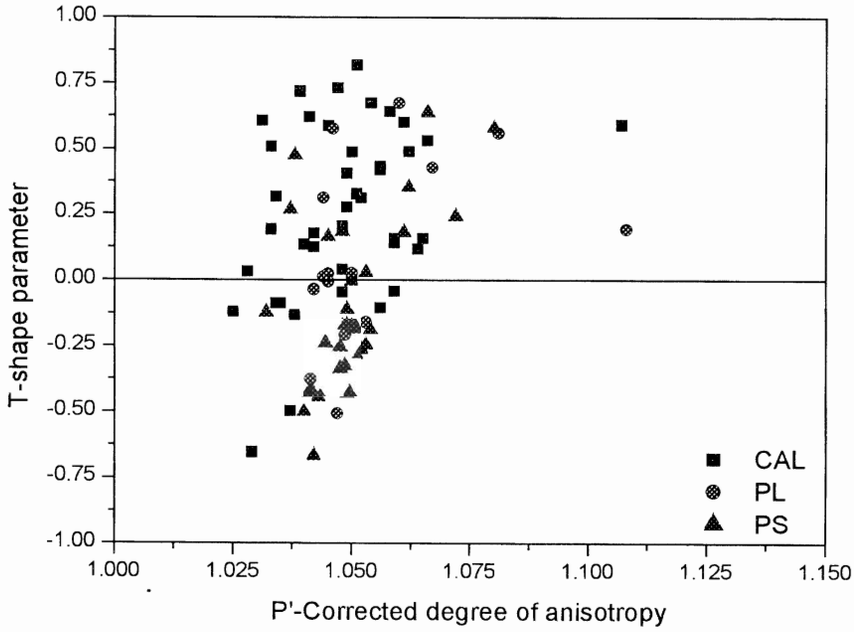

Fig. 9 – JELINEK'S (1981) plot: shape parameter (T) *versus* corrected degree of anisotropy (P') for the three sampled sites.

each site was made using the bi-variate extension (HENRY & LE GOFF, 1995) of Fisher's statistics (FISHER, 1953), which determines the uncertainties on each principal susceptibility direction for all samples of the site. For the computation of the confidence ellipse, we used data weighted using the Fisher's concentration parameters.

The samples analyzed by AMS revealed uniformity of the magnetic carriers, displaying similar characteristics concerning bulk susceptibility values and anisotropy parameters (Figs. 8 and 9).

The observed magnetic susceptibility values for all the samples are low (Fig. 8), typical of granite rocks in

which the paramagnetic and diamagnetic minerals dominate. Analysis of Fig. 8 shows that the magnetic susceptibility values of the three sampled sites are distributed in distinct domains: site PS displays the highest values, with an average of $210 \times 10^{-6} \pm 3.0$ % SI, while site CAL presents the lowest values, $138 \times 10^{-6} \pm 2.5$ % SI; site PL displays an average of $165 \times 10^{-6} \pm 4.1$ % SI.

AMS revealed that there is no dominant shape of the susceptibility ellipsoid, often showing important variations in specimens within the same site. However, it is possible to verify that the samples of site PS show a slight tendency for the prolate shape, while samples from site CAL show a tendency towards the oblate shape (Fig. 9).

The values of the corrected degree of anisotropy parameter (P') range between 2.5 % and 11 %, although most samples fall in the interval between 2.5 % and 7.5 % (Fig. 9).

Stereographic projections (Figs. 10 and 11) show a good clustering of data at sites PL and PS, and appreciable dispersion at site CAL. K_3 (pole of the magnetic foliation) dips approximately 20° to 240 (Tab. 2) in sites CAL and PL, defining a magnetic foliation striking approximately NNW-SE and dipping approximately 70° to the ENE. The K_1 axis, which defines the magnetic lineation, has an average NNW-SSE orientation, gently dipping to the SSE in all sampled sites, parallel to the striations defined by mineral aggregates on the surfaces of the NE-SW faults present in all sites (Tab. 2).

Four spots were sampled along a profile oblique to a subvertical NE-SW fault at site PS (Fig. 11). The distances to the fault, along the profile, were: A – 1420 cm, B – 970 cm, C – 440 cm and D – 50 cm. Data represented in Fig. 11 shows a gradual change of the direction of the K_1 axis and of the foliation with the approximation to the fault. Together, the foliations of the four spots define a zone axis (HENRY, 1997) with attitude 83°, 311. This gentle folding of the foliation is interpreted by us as ductile drag related with the dextral kinematics observed in the fault immediately to the NW.

DISCUSSION AND CONCLUSIONS

Taking into account the age, the geometry and the kinematics of the studied Late Variscan fault pattern, we can conclude that the NNW-SSE and N-S to NE-SW systems are the dextral conjugates of the sinistral ENE-WSW to E-W fault system. AMS data show that maximum compression during granite emplacement was between NE and ENE, compatible with the kinematics and conjugate relationship of the older, Variscan strike-slip faults.

The minor interval between the age of the granite and faulting, and the mineral associations that form the fault infillings suggest that the earlier fracturing took place during granite emplacement and, thus, at relatively high temperatures.

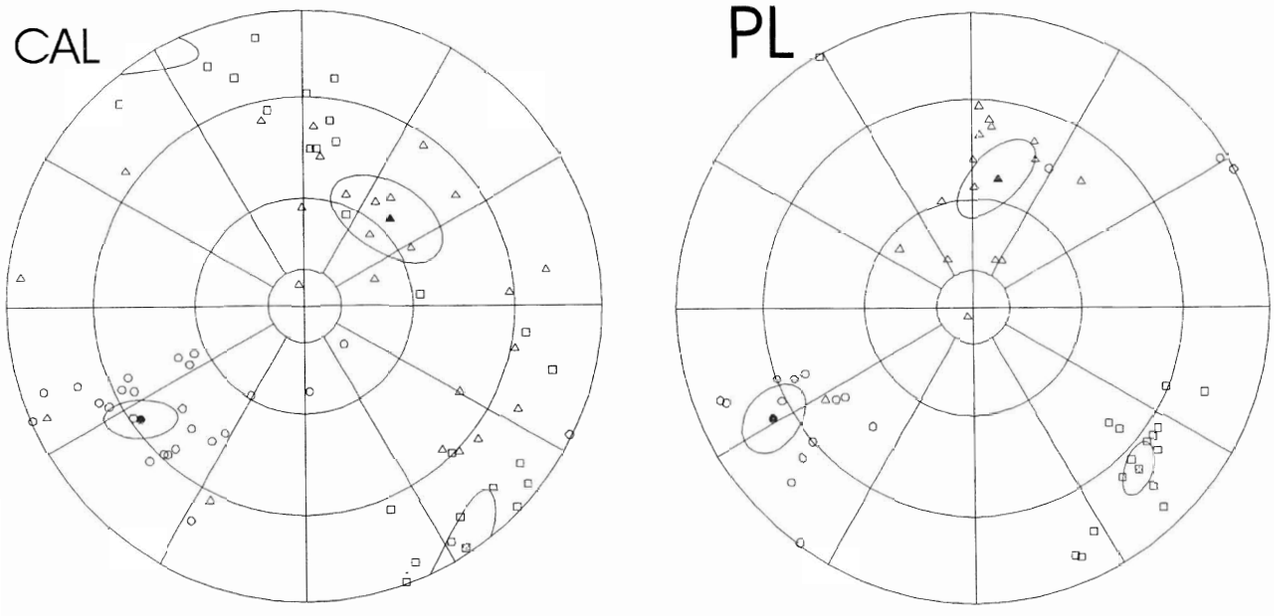

Fig. 10 – Stereographic projections of principal magnetic axis at sites CAL and PL.

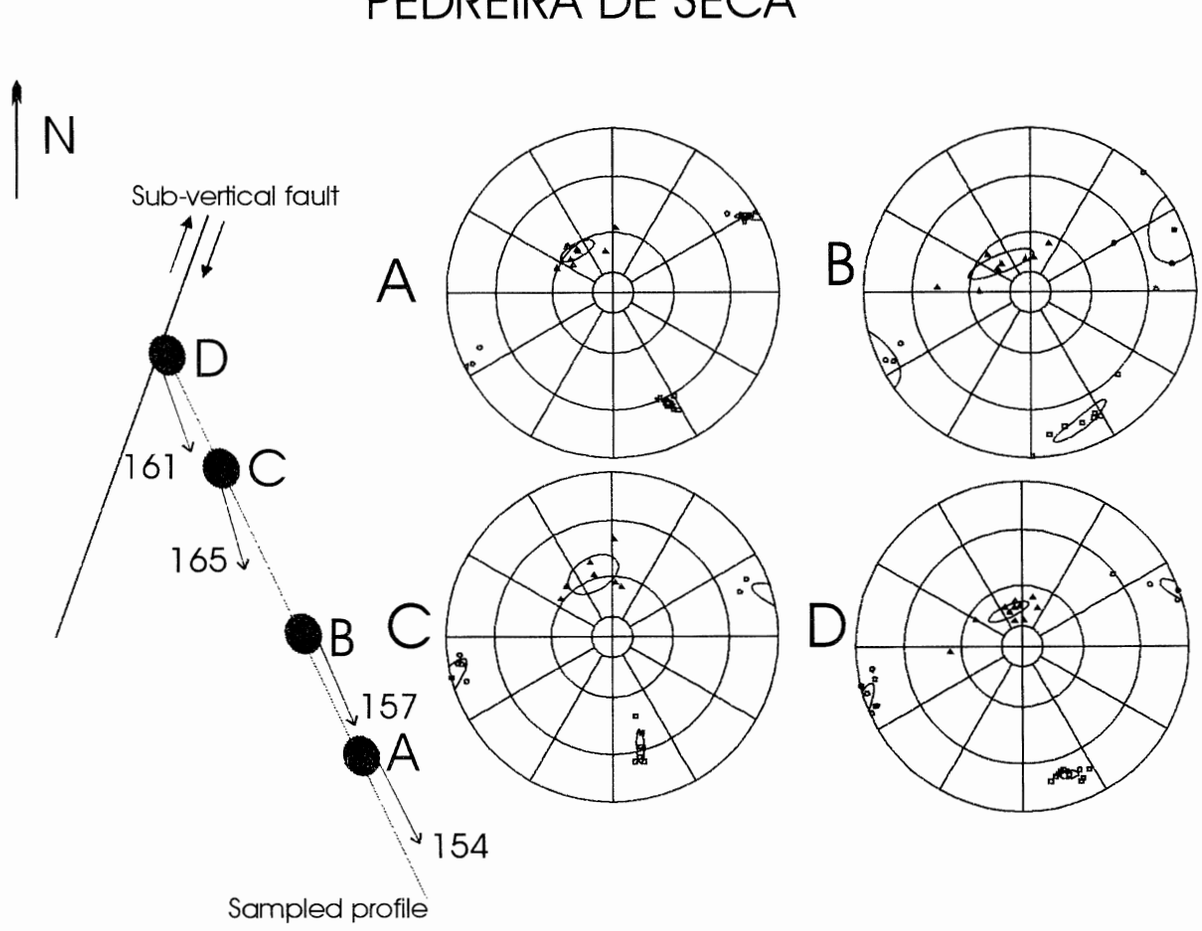

Fig. 11 – Stereographic projections of principal magnetic axis at Pedreira de Seca, together with sketch showing the location of the sampled spots and their relationship with the main sub-vertical NNE-SSW fault zone. Note the gradual variation of the magnetic lineation and foliation along the sampled profile marking the oldest predominant dextral displacement accommodated by the fault.

TABLE 2
Attitudes of the principal axis of the magnetic ellipsoids at each sampled site

Sites	**K_1 (Strike/dip)**	**K_2 (Strike/dip)**	**K_3 (Strike/dip)**
CAL	144/3	43/56	242/21
PL	135/23	10/53	241/23
PS-A	154/27	317/62	60/8
PS-B	157/19	304/66	67/12
PS-C	165/33	340/54	255/1
PS-D	161/19	331/71	70/3

Our data support the conclusion that the Amares basin is a graben – it is an elongate crustal block structurally depressed relative to bordering blocks, and the bordering faults are of near-parallel strike and dip steeply, defining steps along the limiting slopes of the graben. Deep heterogeneous alteration of the granites, controlled by faults, could also explain a topographic depression. But, then, well-preserved flats, limited by faults, in the graben flanks would not be expected. However, they are actually observed and characterize the Amares depression.

The age of crustal uplift and formation of the Amares graben is not yet constrained by palaeontology and sedimentology. However, we can use other indirect evidence to suggest time limits to the main episode of the formation of the Amares graben. We use the preservation degree of geomorphologic features to evaluate the age of the graben, at least the most recent re-activation. As referred above, the well-preserved step-like arrangement of the topography in the slopes bordering the graben (blocks between faults) points towards a recent movement. The graben could not have formed in times older than the upper Miocene, because then the elapsed time would be enough to significantly erase most geomorphologic features, in the absence of a more recent regional uplift and relative subsidence of the graben floor. Even in the case of deep heterogeneous alteration in granites controlled by faults, important recent uplift would have to occur to remove the altered granite.

Comparison between the Amares and the Vilariça grabens with the aim of helping to understand the generation of the former is not possible: one cannot compare dip-slip kinematics (Amares – chocolate tablet strain) with pull-apart basins dominated by strike-slip kinematics. Strike-slip graben in NE Portugal are the result of N-S to NNW-SSE compression that reactivates pre-existing NNE-SSW faults (RIBEIRO, 1984; CABRAL, 1989, 1995; MATEUS *et al.*, 1999; MONTEIRO SANTOS *et al.*, 1999). The same conclusion is not so clear for the stress field responsible for the formation of the Amares graben. Then, what is the possible mechanism responsible for dip-slip movement in all fault systems, *i. e.*, what mechanism could generate extension in two horizontal, orthogonal, directions? Taking into account that the bordering faults are ENE-WSW (graben elongation) and NNW-SSE, both with almost pure dip-slip kinematics, two configurations of the stress field are possible:

1. NNW-SSE horizontal compression due to convergence between the African and the Eurasian plates (DE METS *et al.*, 1990) – such compressive stress could generate large scale ENE-WSW lithosphere buckling, with chocolate tablet strain resulting from extension in the outer-arc.
2. E-W compression in the western Portuguese margin due to incipient subduction (RIBEIRO *et al.*, 1996) – in the absence of large scale lithosphere buckling, such compressive stress would re-activate the NNW-SSE system as sinistral strike-slip and the ENE-WSW system as dextral strike-slip; if there were large scale buckling and extension in the outer arc, the resulting grabens would be elongate N-S.

In view of the above discussion, we favour the first hypothesis. If lithosphere contraction in this region, by the time of formation of the Amares graben, resulted from convergence between the African and the Eurasian plates, then compression would be oriented NNW-SSE and, thus, the NNW-SSE fault system that limits the graben to the W and to the E would not present a strike-slip component, which is the case. Dip-slip kinematics in the ENE-WSW fault system would result from extension in the outer-arc of a large-scale lithosphere buckle. Lithosphere buckling could be a way of accommodating strain to the W of the major Alpine faults of Vilariça and Régua-Verín (where crustal contraction was mostly accommodated by sinistral strike-slip movement – Fig. 12), and could account for the minor reactivation of the NNE-SSW fracture system in the studied area. This hypothesis is to be proved by further regional studies of a more multidisciplinary nature (with Geophysics and Geodesy).

The present study, together with previous studies (MARQUES, 1994; MARQUES & MATEUS, 1998; MATEUS *et al.*, 1999), also shows that the ENE-WSW to E-W fracture system has been in great part neglected in earlier published studies, but is perhaps the most penetrative within the granitic regions. During the sustained rapid (5 to 10 mm/year) Late-Variscan crustal uplift, which is believed to begin at *ca.* 300 Ma (the age of the basal continental conglomerate that marks the Stephanian unconformity is 296 Ma), the rising of the brittle-ductile transition resulted in significant reduction of the crustal strength, since the mechanisms responsible for the generated thermal anomalies occurred much faster than does dissipation of heat by conduction and fluid advection (KOONS, 1987; HOLM *et al.*, 1989; SELVERSTONE *et al.*, 1995). Consequently, the emplacement of late- and post-tectonic granitoids immediately above that mechanical transition occurred at progressively shallower depths, producing also the surface heat flow anomalies required for the pronounced hydrothermal activity associated with the successively reactivated strike-slip faults.

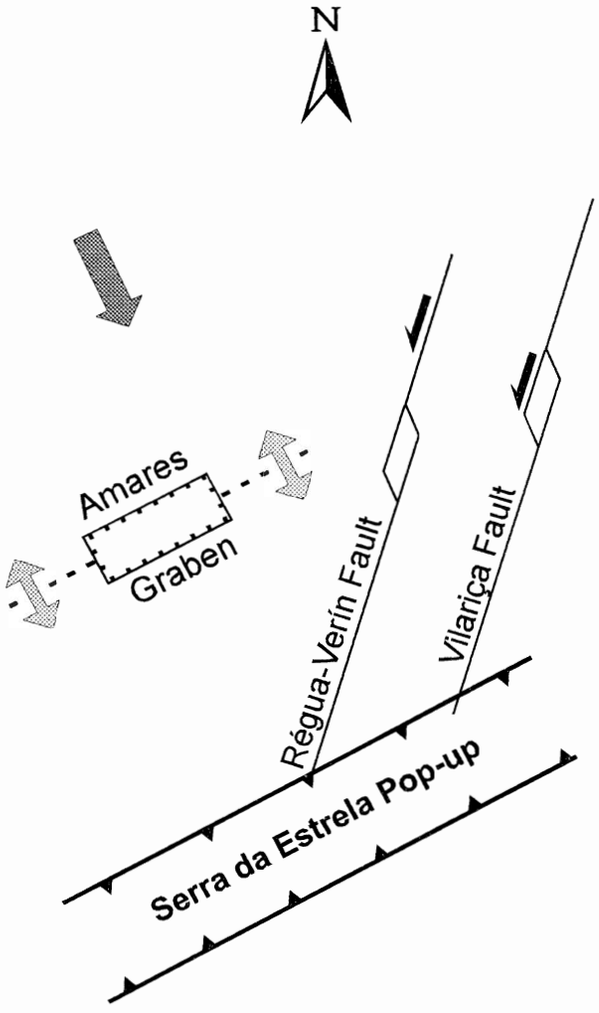

Fig. 12 – Sketch of the tectonic interpretation for the Amares graben in the context of the Alpine deformation affecting the basement of northern Portugal. Double arrows indicate antiformal fold, half arrows strike-slip displacement, and full arrow the direction of the deduced maximum compressive stress.

ACKNOWLEDGMENTS

Fieldwork was supported by FCT through the research project DIWASTE (PRAXIS/P/CTE/11028/1998). AMS analysis was conducted in CGUL Laboratory.

REFERENCES

AMARAL, G.; CORDANI, U. G.; KAWASHITA, K. & REYNOLDS, J. H. (1966) – K/Ar dates of basaltic rocks from southern Brazil. *Geochimica et Cosmochimica Acta*, **30**, pp. 159-189.

CABRAL, J. (1989) – An example of intraplate neotectonic activity, Vilariça basin, Northeast Portugal. *Tectonics*, **8**, pp. 285-303.

CABRAL, J. (1995) – A Neotectónica em Portugal Continental. *Mem. Serv. Geol. Portugal*, Nova Série, Vol. **31**.

CABRERA, L.; FERRÚS, B.; SÁEZ, A.; SANTANACH, P. F. & BACELAR, J. (1996) – Onshore cenozoic strike-slip basins in NW Spain. In: Friend, P. F. and Dabrio, C. J. (Eds.), *Tertiary basins of Spain: the stratigraphic record of crustal kinematics*. Cambridge University Press, pp. 247-254.

DEMETS, C.; GORDON, R. G.; ARGUS, D. F. & STEIN, S. (1990) – Current plate motions, *Geophys. J. Int.*, **101**, pp. 425-478.

FISHER, R. A. (1953) – Dispersion on a Sphere. *Proc R. Soc. Lond.*, A**217**, pp. 295-305.

HENRY, B. & LE GOFF, M. (1995) – Application de l'extension bivariate de la statistique de Fisher aux données d'anisotropie de susceptibilité magnétique: intégration des incertitudes de mesure sur l'orientation des directions principales. *Compt. Rend. Acad. Sci. Paris*, **320**, II, pp. 1037-1042.

HENRY, B. (1997) – The magnetic zone axis: a new element of magnetic fabric for the interpretation of the magnetic lineation. *Tectonophysics*, **271**, pp. 325-329.

HOLM, D. K.; NORRIS, R. J. & CRAW, D. (1989) – Brittle and ductile deformation in a zone of rapid uplift: central southern Alps, New Zealand. *Tectonics*, **8**, pp. 153-168.

JELINEK, V. (1981) – Characterization of the magnetic fabric of rocks. *Tectonophysics*, **79**, pp. 63-67.

KOONS, P. O. (1987) – Some thermal and mechanical consequences of rapid uplift: an example from the southern Alps, New Zealand. *Earth and Planetary Science Letters*, **86**, pp. 307-319.

MARQUES, F. O. (1994) – *Estudo Tectónico das Rochas Infracrustais do Manto de Soco do SW do Maciço de Bragança (Trás-os--Montes)*. Ph. D. Thesis, Universidade de Lisboa.

MARQUES, F. O. & MATEUS, A. (1998) – Have NNE-SSW transcurrent shear zones always been sinistral in the Variscan basement?. *4.ª Conf. Anual do Grupo de Geologia Estrutural e Tectónica*, Porto, *GEOlogos*, **2**, pp. 73-76.

MARTÍN-SERRANO, A.; MEDIAVILLA, R. & SANTISTEBAN, J. I. (1996) – North-western Cainozoic record: present knowledge and the correlation problem. *In*: Friend, P. F. and Dabrio, C. J. (Eds.), *Tertiary basins of Spain: the stratigraphic record of crustal kinematics*. Cambridge University Press, pp. 237-246.

MATEUS, A. (1995) – *Evolução Tectono-térmica e Potencial Metalogenético do Troço Transmontano da Zona de Falha Manteigas-Vilariça-Bragança*. Ph. D. Thesis, Universidade de Lisboa.

MATEUS, A.; ANDRADE, M.; CABRAL, J. & MONTEIRO SANTOS, F. (1999) – Análise cinemática e dinâmica da rede de fracturas identificada na região de Sta Comba da Vilariça – Pocinho (NE Portugal). *5.ª Conf. Nacional do Grupo de Geologia Estrutural e Tectónica*, Vila Real, pp. 18-25.

MATEUS, A.; RIBEIRO, A. & BARRIGA, F. J. A. S. (1995) – Pore fluid and seismogenic characteristics of fault rocks within the Vilariça Fault Zone (NE Portugal): evidences for deep fluid circulation during the uplift of the Variscan continental crust. *Mem. Museu Lab. Mineral. Geol. Univ. Porto*, **4**, pp. 281-285.

MONTEIRO SANTOS, F.; MATEUS, A.; MATOS, L. & CABRAL, J. (1999) – Modelação numérica de bacias transtensionais; ensaio de aplicação à depressão de Vilariça (NE Portugal). *5.ª Conf. Nacional do Grupo de Geologia Estrutural e Tectónica*, Vila Real, pp. 26-31.

PEREIRA, E.; IGLÉSIAS, M. & RIBEIRO, A. (1984) – Leucogranitos – "stockscheider" e o controlo estrutural da mineralização na mina de Montesinho – Bragança. *Comun. Serv. Geol. Portugal*, **70**, pp. 11-22.

PEREIRA, E.; RIBEIRO, A. & MEIRELES, C. (1993) – Cisalhamentos hercínicos e controlo das mineralizações de Sn-W, Au e U na Zona Centro-Ibérica, em Portugal. *Cuaderno Lab. Xeolóxico de Laxe*, Coruña, **18**, pp. 89-119.

RIBEIRO, A. (1974) – Contribution à l'étude tectonique de Trás-os--Montes oriental. *Mem. Serv. Geol. Portugal*, vol. **24**.

—— (1984) – Néotectonique du Portugal. *Livro de Homenagem a O. Ribeiro*, Centro de Estudos Geográficos, pp. 173-182.

RIBEIRO, A.; ANTUNES, M. T.; FERREIRA, M. P.; ROCHA, R. B.; SOARES, A. F.; ZBYZEWSKI, G.; ALMEIDA, F. M.; CARVALHO, D. & MONTEIRO, J. H. (1979) – *Introduction à la Géologie Génerale du Portugal.* Serviços Geológicos de Portugal, Lisboa.

RIBEIRO, A.; CABRAL, J.; BAPTISTA, R. & MATIAS, L. (1996) – Stress pattern in Portugal mainland and the adjacent Atlantic region, West Iberia. *Tectonics*, **15**, pp. 641-659.

RIBEIRO, A.; PEREIRA, E. & SEVERO, L. (1980) – Análise da deformação da zona de cisalhamento Porto-Tomar na transversal de Oliveira de Azeméis. *Comun. Serv. Geol. Portugal*, **66**, pp. 3-9.

SELVERSTONE, J.; AXEN, G. J. & BARTLEY, J. M. (1995) – Fluid inclusion constraints on the kinematics of footwall uplift beneath the Brenner Line normal fault, eastern Alps. *Tectonics*, **14**, pp. 264-278.

STEIGER, R. H. & JAGER, E. (1977) – Sub-commission on geochronology: convention on the use of decay constants in geo- and cosmochronology. *Earth Planetary Science Letters*, **36**, pp. 359-362.

TARLING, D. H. & HROUDA, F. (1993) – The Magnetic Anisotropy of Rocks. *Chapman & Hall.*

Artigo recebido em Abril de 2001